Effects of resistive windscreens and foam inserts on the acoustic response of an in-flow phased microphone array

W. Clifton Horne*, Nathan J. Burnside** - *NASA Ames Research Center*

Stephen D. Schery† - *Aerospace Computing, Inc*

Gary G. Podboy†† -*NASA Glenn Research Center*

Christopher J. Bahr+, Daniel J. Stead++, William M. Humphreys§
NASA Langley Research Center

Submittal Abstract for 2021 AIAA SciTech Forum, 11-15 January 2021
Presentation category: Aeroacoustics- Advanced Measurement Methods

Symbols:

θe – source emission angle, deg. This is also the array reception angle.
θm – source measured angle, deg = θe at M = 0
M – Mach no.
c - sonic speed
CBF – conventional (delay-and-sum) beamform
CSM – array cross-spectral matrix
C_R – reflection coefficient
C_{RN} – normal reflection coefficient
C_{WS} – windscreen correction = $20*\log(2*p_I / p_0)$; the factor of 2 cancels the pressure doubling of effect of the plate. Experimentally, C_{WS} = Lp(free-field mic)+ 6 dB – Lp(array CBF peak)
D = recess depth of microphone plate behind the windscreen
f – frequency
k – wavenumber = 2*pi*f/c
p_F = sound pressure in front of the windscreen, $p_F = p_I + p_R$
p_B = sound pressure behind the windscreen
p_I = incident sound pressure
p_R = reflected sound pressure
p_0 = sound pressure on microphone plate
Rs = screen steady flow resistance in Pa/(m/s) or MKS Rayls
U_S = acoustic particle velocity normal to the screen

---

* Aerospace Engineer, Associate Fellow AIAA
** Aerospace Engineer, Senior Member AIAA
† Principal Scientist
†† Research Engineer, Member AIAA
+ Senior Research Engineer, Associate Fellow AIAA
++ Senior Engineer
§ Senior Aerospace Technologist, Associate Fellow AIAA

SS325x325 – stainless steel screen material, 325x325 wires/ in., plain weave
SS200x600 – stainless steel screen material, 200x600 wires/in. , dutch twill weave
SS165x800- stainless steel screen material, 165x800 wires/in., dutch twill weave
Kevlar120 – Kevlar screen material, 1.8 oz/yard, 34 x 34 strands/in open weave
Z = screen-plate impedance
Z_N = normal incidence screen-plate impedance
ρ = fluid density

Background and objectives of the studies

Phased microphone arrays are employed in both open-jet and closed test-section wind tunnel aeroacoustic research facilities to determine the locations and levels of noise sources associated with a wide variety of novel flight vehicle configurations. When used in a closed test section, the in-flow microphone array is subject to background noise sources including hydrodynamic pressure fluctuations from the turbulent boundary layer over the array surface. Several approaches to reduce this noise have been successfully demonstrated, including increasing the number of flush-mounted microphones to improve signal-to-noise ratio[1], as well as recessing the microphones behind a porous windscreen such as Kevlar[2] , stainless steel[3,4] , or with porous foam by itself [5] or in the cavity[4] between the windscreen and array plate.

This report will present results from several recent research studies that were conducted to optimize the windscreen approach with respect to maximizing the signal to flow-noise ratio of the in-flow array while minimizing the uncertainties and errors in measuring acoustic levels of the target sources of interest. These studies at NASA's Ames(ARC), Glenn(GRC), and Langley(LaRC) Research Centers utilized the same basic array design consisting of a streamlined fairing with a circular array plate recessed beneath a windscreen installed in the fairing upper surface[6]. The effects of adding resistive foam to the cavity between the windscreen and array plate were also studied. The array microphone plates were recessed behind a porous windscreen fabricated of either Kevlar 120 cloth, or stainless steel screens with a variety of screen weave densities and normal flow resistances. This array concept has been tested previously to validate the design and results of in-flow measurements from a variety of reference acoustic sources have been reported[6,7].

The objectives of the studies of this report were to understand and systematically quantify the effects of the windscreen design and cavity treatments on the response of the array to low frequency background noise due to turbulent flow over the windscreen, and on the modification of the acoustic sensitivity to in-flow acoustic sources. The acoustic sources and corresponding array responses were characterized in a variety of wind tunnels and an anechoic chamber over a wide bandwidth (0.5 to 100 kHz) and range of emission angle (0˚ to 180º).

Description of test hardware

The arrays used in these studies were of the same design, consisting of an 8 in. diameter, 3-arm spiral pattern[1] of 24 microphones mounted in an aerodynamic fairing 14 in. wide and 21 in. long. The fairing was 2 in. deep for the ARC and GRC configurations. The test at LaRC also used an

8” diameter pattern with 33 microphones in the same relative locations as the out-of-flow, open-frame SADA array used in the LaRC Quiet Flow Facility[8] and this fairing was made 3 in. deep to accommodate the microphones. The fairing was designed to be mounted on an airfoil strut above the wall boundary layer to M=0.33 and has been tested in a number of wind tunnel facilities to M=0.3. In the results presented here, the microphones were either B&K or G.R.A.S ¼” condenser microphones mounted with the grids removed and diaphragms flush with the plate. The plate was recessed 0.5 in. beneath the windscreen and used with and without a foam insert in the cavity between the plate and the screen.

The tests at ARC and LaRC used in-flow acoustic sources consisting of a 2 in. diameter sphere (airball) with 44 microjets on the outward facing hemisphere[6,7]mounted in an aerodynamic fairing of the same design as used for the array and a usable broadband output of 0.5 to 100 kHz. The LaRC test also measured the response to steerable tweeters (0.7-40 kHz) mounted in the source fairing. The in-flow acoustic source for the GRC test was an open pipe connected to an external driver located outside of the tunnel wall. Fig. 1 presents photographs of the array and acoustic source configurations of the study.

At ARC, microphone data were acquired with National Instruments 24 bit A/D and a bandwidth of at least 100 kHz. Data from the GRC test were acquired with a HBM Gen3i Data Acquisition Recorder. BeamformInteractive software from Optinav was used to generate source location maps and beamformed spectra. Custom array processing software developed by NASA was also used.

Description of development and optimization tests:

The following table lists the research tests that provided measurements to be reported in this study:

Table 1. List of in-flow array windscreen optimization studies

Description	Facility	Emiss. Ang.	Lateral dist	Mach No	screen, treatments
S1) screen/foam resistance	ARC FML screen resistance calibrator	N/A	N/A	0.1-1.4 m/s	Kevlar120, s. steel(5), foam(4)
S2) screen reflection coeff., acoust. model	ARC FML impedance tube	90˚	N/A	0	Kevlar120, stainless steel(3)
S3) array static response	ARC Anechoic Chamber	0˚-180˚	42, 48 in.	0	Kevlar120, s. steel(5), foam(4)
S4) array in-flow response	GRC 9x15-ft Wind Tunnel	90˚	42 in	0.2	s.steel(3), foam(6)
S5) array in-flow response	Army 7x10 ft Wind Tunnel(ARC)	54˚-142˚(7)	48 in.	0 - 0.25(4)	Kevlar120, s.steel(4), foam(1)
S6) array in-flow response	LaRC Quiet Flow Facility	45˚-135˚(7)	24 in.	0-0.17(6)	s.steel(1), foam(1)

The test setups in the Army 7-by10-ft Wind Tunnel(S5) and the ARC anechoic chamber (S3) are shown in Fig. 2 and 3 respectively. Fig. 4 and 5 show the corresponding set-ups in the GRC 9-by 15-ft Wind Tunnel and the LaRC Quiet Flow Facility. The main topics of this report are the measurements of the effects of wind screen material resistance on suppression of low frequency background noise in each wind tunnel, and a comparison of measurements of static array acoustic response with various windscreen treatments to a recently developed acoustic model of

the effects of a simple resistive screen. Further results, such as detailed effects of forward speed on array acoustic response, recommendations of optimal windscreen design, calibration and correction methods, and quantification of the signal-to-noise ratio and level measurement accuracy of the optimal designs will be reported at a later date.

Results of research studies

Flow resistance of windscreen and cavity foam materials

Four windscreen materials and one cavity foam were selected for full evaluation of acoustic effects on array performance, as listed in the table below. These were selected from a larger list of over 20 screen materials and foams.

Table 2. Windscreen and cavity foam materials reported in this study.

Material and weave (thread/in)	Wire/fiber diam(in)	MKS Rayls (Pa/(m/s)
Kevlar120 (1.8 oz/yard, 34x34	0.0035	70-200
stainless steel 304, 325x325	0.0014	25
stainless steel 304, 200x600	0.002/0.0018	80
stainless steel 304, 160x800	0.003x0.002	165
P30 foam	30 pores/in	~20

The steady flow resistance of each windscreen material was measured in the plenum of a modified hot-wire calibrator in which the flow rate was measured with a pitot probe at the calibrator nozzle exit, as shown in Fig. 6. Resistance measurements of samples of the same material from different batches were repeatable to within 2-3%. The three stainless steel screens exhibit a nearly linear variation of flow resistance vs velocity, while the Kevlar120 has a nearly quadratic variation. This admits the possibility that the Kevlar acoustic effects may be amplitude dependent, and that harmonic distortion may also be present with this screen. The sound pressure levels associated with three velocities are indicated on the graph. For example, a rms velocity of 0.4 m/s is associated with an acoustic level of 138.4 dB.

Effect of windscreen resistance on low frequency noise suppression and broadband frequency response

Fig. 7 shows the PSD spectra from the array with the 24-microphone pattern in the GRC 9-by 15-Foot Wind Tunnel at M = 0.2 with three different stainless steel screens, and with (right) or without (left) P30 foam in the ½" deep cavity between the array plate and the windscreen. The spectra represent the average of the 24 CSM diagonal elements (autospectra). The cavity foam attenuates low frequency noise to some degree below 1 kHz. In each figure, the spectrum from a freefield microphone in the same location as the array screen center at M= 0 is shown as a red line and depicts the level of the active sound pipe in the acoustically treated test section. Below 4-5 kHz, the wind-on spectra are dominated by low frequency noise due to the turbulent boundary layer above the array screen. The levels and roll-off rates with frequency are strongly dependent on the screen resistance, and can be approximated by the empirical curve fit:

$$PSD_{Low\ Freq<5\ kHz} = 48 - 37 * \log[Rs(cgs\ Rayls)] - 67.5 * \log\left[\frac{5}{Freq(kHz)}\right]$$

Fig. 8 shows 1/12th octave spectra from the array (CBF peak level) with the 24-microphone pattern in the Army 7-by 10-Ft Wind Tunnel for the conditions of M = 0.208, source angle θm of 69.7˚ and four windscreen materials. The left plot of Fig. 8 shows that below 1 kHz, the beamforming computed reliable results for the SS200x600, SS165x800, and Kevlar120 windscreens, but not for the SS325x325 screen. Between 1 kHz and 5 kHz, the background levels exhibit a similar trend of decreasing background noise level with increasing windscreen resistance, but to a lesser degree compared the PSD spectra of Fig. 7. Variations in background noise level are also seen above 5 kHz, such as a broad peak in the Kevlar 120 spectra from 25 to 40 kHz consistent with previously reported results[7].

The right plot in Fig. 8 shows similar 1/12th octave spectra from the array with the airball source active at 16.5 psi source pressure. The background noise is unchanged below 4 kHz compared to Fig. 8 left plot. Above this frequency, the spectra are dominated by the signal from the airball source. The response spectra from the stainless steel windscreens are comparable to within a few dB, however the response spectrum from the Kevlar windscreen exhibits a noticeable attenuation of 2-3 dB from 6 to 18 kHz and resonance peaks of about -5dB above that frequency. This plot also illustrates the low output level of the airball source below 5 kHz that has been improved in a previous study with the use of a ducted compression driver to the airball fairing[7] with results similar to the sound pipe used in the GRC test reported here.

As described previously[2,3] and above, resistive windscreens (without foam) affect broadband acoustic response in the form of resonances that vary with emission angle and frequency. Fig. 9 presents windscreen correction (C_{WS}) contour maps in dB for the SS325x325 windscreen, with linear frequency (0-100 kHz) on the horizontal axis and emission angle (0˚ to 180˚) on the vertical axis. The left plot is for windscreen alone and the right plot is windscreen + foam (different than P30). The foam appears to damp out some of the resonance peaks but also imposes a significant correction level dependence on frequency and emission angle. Note that the overall variation in C_{WS} for screen+foam is significantly larger than for the screen alone. These maps were obtained in the ARC anechoic chamber with a set-up similar to that shown in Fig.3, except with the array on the turntable.

Fig. 10 shows similar windscreen correction contour plots for the Kevlar windscreen over 24-microphone pattern arrays that are 8 in. diameter (left) and 23 in. diameter(right) with the airball source distance = 48 in. using data from a previous test.[7] Note that the resonant peak frequencies are comparable to the previous case for SS325x325. The resonant peak amplitudes in C_{WS} above 20 kHz are significantly larger than for the SS325x325 windscreen and grow in amplitude with frequency. Kevlar windscreens are in use for research tests at ARC, but primarily for lower frequency measurements below 20 kHz. The variation in C_{WS} resonant peak level is similar for the two arrays at 90˚ angle but decreases more with emission/reception angle away from 90˚ for the larger array relative to the smaller. This calibration distance effect needs to be taken into account if the ratio of array diameter to calibration distance is larger than a nominal value and the calibration source distance is different from the distance from array to source in the wind

tunnel test. In the following section, we will establish that the 48" calibration source distance was sufficiently large to render the distance effects negligible for the 8" diameter array pattern.

Fleury[3] developed a useful extrapolation of the windscreen correction from the measured correction spectrum at 90˚ reception:

1) $C_{WS}(\theta e,f)= C_{WS}(90^{\circ},f*\sin(\theta e))$.

Figure 11 shows four plots of windscreen correction, C_{WS}, for SS200x600 from the ARC anechoic chamber measurements with 48" airball source distance. The upper left figure a) shows the original full correction map measured at 5˚ increments from 0˚ to 180˚. The upper right plot b) shows the $1/12^{th}$ octave C_{WS} spectrum (dashed red line) at 90˚ reception(emission) angle. The solid black line is a cubic spline interpolation, but the narrow-band spectrum could also be used. The lower left plot c) is a map of C_{WS} extrapolated from the 90˚ spectrum using Fleury's method. This extrapolation is accurate near 90˚ but does not decay with angles further away from 90˚ as does the full correction map (upper left). The lower right C_{WS} map d) is also extrapolated from 90˚ spectrum with an added term:

2) $C_{WS}(\theta e,f)= \sin(\theta e)*C_{WS}(90^{\circ},f*\sin(\theta e))$

This map differs from the original map by 0.5 dB or less for most of the range of frequencies and emission angles, due mostly to the fact that the extrapolated map is smoother. This agreement is consistent with the correction 2) for a source effectively at infinite distance, as noted previously, since distance is not a factor in this extrapolation. An accurate extrapolation method for C_{WS} can be advantageous for correcting windscreen effects to arbitrary emission angles in comparison to a 2D interpolation of the full C_{WS} map.

Figure 12 presents correction spectra at 90˚ for the three stainless steel screens with and without P30 foam in the cavity. The resonance peak amplitudes in the mid- to upper-frequency range (20-100 kHz) for the SS325x325, SS200x600, and SS165x800 screens are approximately 0.5 dB, 1.2 dB, and 2 dB respectively. The noisy and non-sinusoidal shape of C_{WS} in these plots at low frequencies is likely due to low sound levels from the airball in this range and could be improved with a more energetic low-frequency source such as a loudspeaker. There is also a small (< 0.5 dB) half-cycle variation of the mean correction level (without foam) over the full frequency range. The effect of the foam is to decrease the resonance amplitude by about half (in dB) as well as an overall correction of about +2 dB, but these effects are not consistent over frequency or screen resistance. Figs. 11 and 12 suggest that the screen-alone effects may be more repeatable, and easier to model and correct without adding the foam.

Development of a simple screen-correction model

Expressions for the impedance and reflection coefficient of a porous resistive screen suspended over a reflecting plate have been published previously[9,10]. From these expressions, the impedance and reflection coefficients for normal incidence ($\theta e=90^{\circ}$) are:

3) $Z_N = R_S - i\rho c * \cot(kD)$, for an incident wave moving in the + x direction, screen at x = -D, and microphone plate at x = 0.

4) $$C_{RN} = \frac{p_R}{p_I} = \frac{Z_N - \rho c}{Z_N + \rho c} = \frac{R_S - i\rho c \cot(kD) - \rho c}{R_S - i\rho c \cot(kD) + \rho c}$$

The acoustic particle velocity in front of the screen is equal to the velocity through the screen:

5) $$U_S = \frac{p_I(1 + C_{RN})}{Z_N} = \frac{p_I(1 + C_{RN}) - p_B}{R_S}$$

The standing wave between the screen and the plate relates the pressure behind the screen to that on the plate:

6) $$\frac{p_B}{p_0} = \cos(kD)$$

Combining equations 5) and 6) gives an expression for the ratio of the incident pressure to the plate pressure:

7) $$\frac{p_I}{p_0} = \frac{\cos(kD)}{\left[(1 + C_{RN})\left(1 - \frac{R_S}{Z_N}\right)\right]}$$

This ratio can also be adapted for the case of arbitrary incidence or extrapolated to other emission angles using equation 2). This expression is not intended to replace the experimental approach described earlier for obtaining the wind screen correction but can be used to model effects of variations in cavity depth and screen resistance on acoustic response, to optimize array designs and characterize measurement uncertainty.

Fig. 13 compares the predicted normal reflection coefficient from equation 4) with measurements of the screen materials obtained from a B&K 4002 impedance tube, with three different sound levels (differentiated by symbol) measured at the base plate. With a 4 in. diam impedance tube, the measurements were accurate up to 1800 Hz. For this study, the screen was positioned 4 in. in front of the base plate, so resonant peak frequencies were 8 times lower than for the array depth of 0.5 in. The predictions were based on the steady flow resistance presented in Fig. 6. The measured reflection coefficients of the stainless steel screens compared well with the predicted values independent of the amplitude. Ratios of pressures measured in front of ($p_F = p_{I+} p_R$) and behind the screen (p_B), as well as at the plate(p_0) also agreed well with predictions. The Kevlar screen exhibited variations with calibration amplitude as noted in the discussion of Fig. 6, as well as more scatter at each of the two amplitude settings shown.

Fig. 14 compares predicted vs measured magnitudes and phases of the a) reflection coefficient , b) p_B/p_F, c) p_0/p_F, and d) 20*log(magnitude) and phase of the windscreen correction $2*p_I/p_0$ for the SS200x600 screen. The magnitude of the predicted resonant peak correction in dB is about 0.75 dB compared with an estimate of 1.2 dB from Fig. 12 of the measured value for this screen. The difference in resonant peak magnitudes may be due to a higher screen resistance at non-zero frequencies than measured for steady flow, or for other causes currently being studied. Fig. 14d also shows a predicted array measurement phase error of about +/- 0.9 rad or +/-5 deg. Phase variation with frequency that increase with screen resistance can be a consideration for accurate time-domain beamforming of sources such as rotor or propeller noise.

Concluding Remarks

The effects of varying windscreen resistance and cavity foam treatments on the acoustic response of an in-flow phased microphone array have been characterized by recent experiments at ARC, GRC, and LaRC using common array and calibration source designs. Analyses of results from these tests are ongoing, however some initial findings include:

- Windscreen resistance, measured as pressure drop for a steady flow velocity normal to the screen, affects suppression of low frequency flow noise and introduces cavity resonances in the array response. The resonances are consistent with predictions from a simple acoustic model based on the reflection coefficient of the screen + cavity.

- A screen resistance of 25 MKS Rayls (SS325x325) was not sufficient to suppress flow noise below 1kHz for successful conventional beamform array processing at M = 0.208. A screen resistance of 80 MKS Rayls (SS200x600) or higher allowed array processing below 1 kHz.

- Extrapolation of the windscreen correction over the full range of reception angles as proposed by Fleury can be improved by including an additional sin(θe) factor to his proposed correction.

- Fine mesh stainless steel screen has a nearly linear steady flow resistance with velocity and negligible amplitude effect on the reflection coefficient. Kevlar120 has a nearly quadratic flow resistance with velocity and exhibits noticeable variations of reflection coefficient depending on calibration amplitude.

These results will be used to improve and optimize array designs, to develop effective calibration procedures, and to improve the accuracy of array measurements in future aeroacoustic research studies.

We anticipate that the final paper and presentation will benefit from further analyses of the data from the tests including data that has been delivered from GRC and LaRC but not yet processed. We also hope to obtain further measurements of windscreen phase corrections and of the effects of calibration distance and source amplitude with stainless steel and Kevlar windscreens.

Acknowledgement

This study was supported by NASA's Aeronautical Research Mission Directorate (ARMD) Advanced Air Transport Technology Project (AATT).

References

1. Underbrink, J., "Aeroacoustic Phased Array Testing in Low Speed Wind Tunnels", in Aeroacoustic Measurements, T. Mueller, ed., Springer 2002.

2. Jaeger, S., Horne, W., and Allen, C., "Effect of Surface Treatment on Array Microphone Self Noise", AIAA-2000-1937, 6th AIAA/CEAS Aeroacoustics Conf. and Exhibit, 12-14 2000, Lahaina, HI.

3. Fleury, V., "Optimization of Microphone Array Wall Mountings in Closed-Section Wind Tunnels", AIAA Journal, v. 50, no. 11, Nov. 2012.

4. Szöke, M., and Azarpeyvand, M, "Reduction of the Hydrodynamic Noise on a Beamforming Array", BeBeC-2016-D2, 7th Berlin Beamforming Conference, 29 Feb. – 1 Mar, 2016, Berlin, Germany.

5. Dougherty, R., "Directional Acoustic Attenuation of Planar Foam Rubber Windscreens for Phased Arrays", BeBeC-2012-0, Berlin Beamforming Conference, 2012.

6. Horne, W.C., and Burnside, N.J., "Initial Calibrations and Wind Tunnel Test Results for an In-Flow Reference Array using New In-Flow Acoustic Sources in Four Array Mount Configurations", AIAA-2018-2969, 2018AIAA/CEAS Aeroacoustics Conf., 25-29 June 2018, Atlanta, GA.

7. Horne, W., and Burnside, N., "Measurements of the Effects of Array Pattern Size and Windscreen Material on the Performance of a Wall-mounted Phased Microphone Array in a Hard-wall Wind Tunnel Using Enhanced In-flow Reference Sources", AIAA-2019-2411, 25th AIAA/CEAS Aeroacoustics Conf., Delft, NL, 20-23 May 2019.

8. Brooks, T., and Humphreys, W., "Effect of Directional Array Size on the Measurement of Airframe Noise Components", AIAA-99-1958, 5th AIAA/CEAS Aeroacoustics Conf. and Exhibit, Bellevue, WA, 10-12 May, 1999.

9. Pieren, R., "Sound Absorption Modeling of Thin Woven Fabrics Backed by an Air Cavity", Textile Research Journal, 82(9) 864–874, 2012.

10. Morse and Ingard, Morse and Ingard, Theoretical Acoustics, McGraw-Hill, 1968, p. 304.

Array patterns

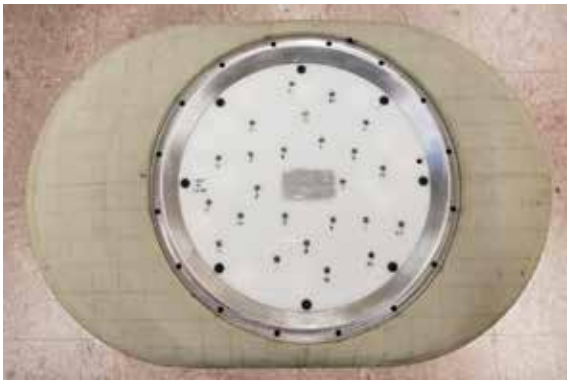

a. ARC 24/25 element 3-arm spiral array pattern

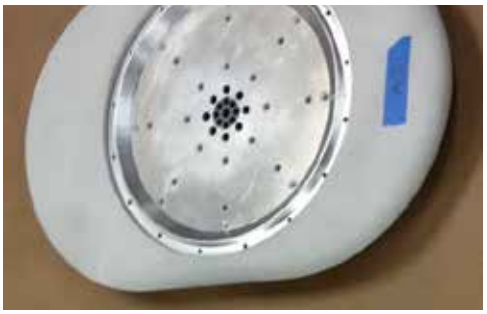

b. LaRC 33 element SADA pattern

In-flow calibration sources

c. multi-jet hemisphere (airball)

c. two steerable tweeters

Fig. 1. In-flow array and reference source configurations.

Fig 2. Array and source set-up in test section of Army 7-by10-Ft Wind Tunnel at ARC.

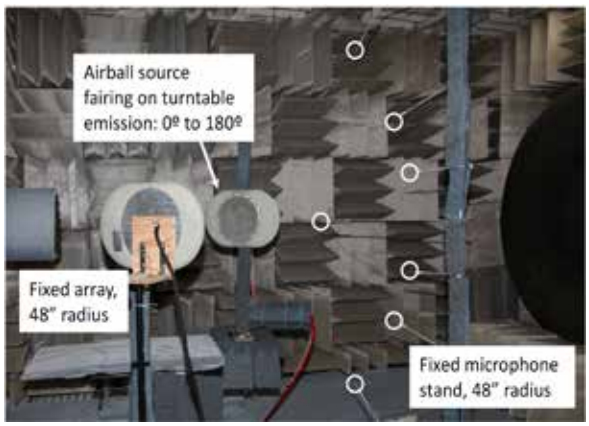

Fig. 3. Array, fixed microphone stand, and source set-up in ARC anechoic chamber.

Fig 4. Array and sound source Set up in GRC 9-by15-Ft Aero-Acoustic Wind Tunnel.

Fig. 5. Array and source fairings mounted on sidewalls of the LaRC Quiet Flow Facility nozzle.

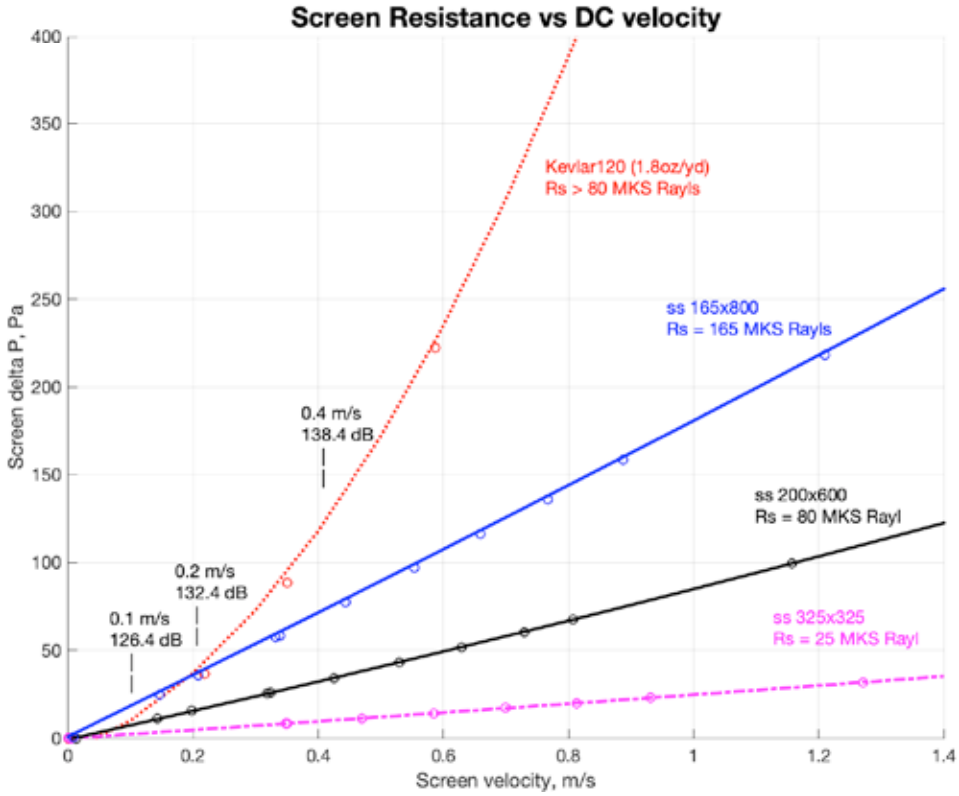

Fig. 6. Steady flow resistance of four windscreen materials vs steady flow velocity.

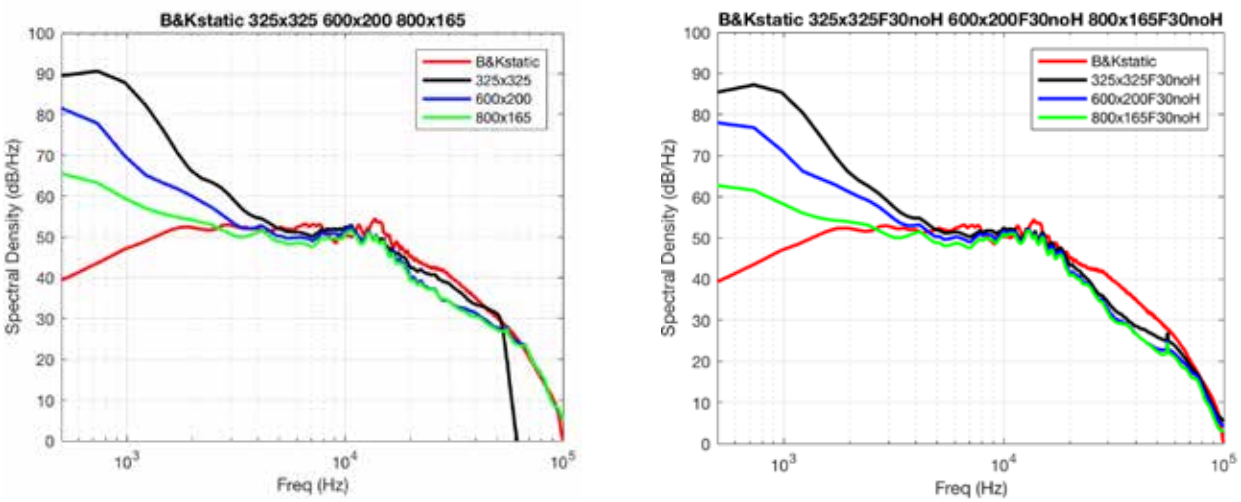

Fig. 7 PSD sound levels (average of CSM diagonal elements) at M=0.2
(left) GRC 9-by 15-Ft Wind Tunnel sound tube source, stainless steel windscreens
(right) stainless steel windscreens + ½" thick P30 foam. The red curves are ¼" free-field microphone at M=0.

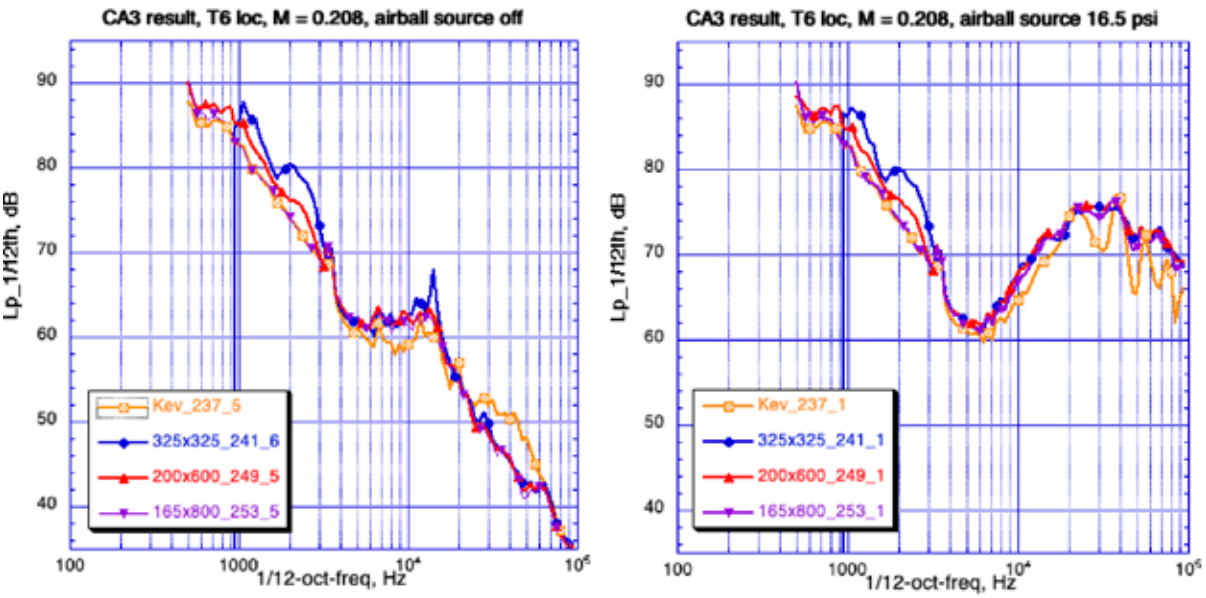

Fig. 8. Array 1/12th octave conventional beamform peak uncorrected spectra from ARC 7- by 10-Ft Wind Tunnel test of 24 element array with four windscreen materials, M = 0.208: Kevlar(gold), SS325x325(blue), SS200x600(red), and SS165x800(violet).
(left) airball source off, (right) airball source 16.5 psi(max). Source lateral distance = 60 in.

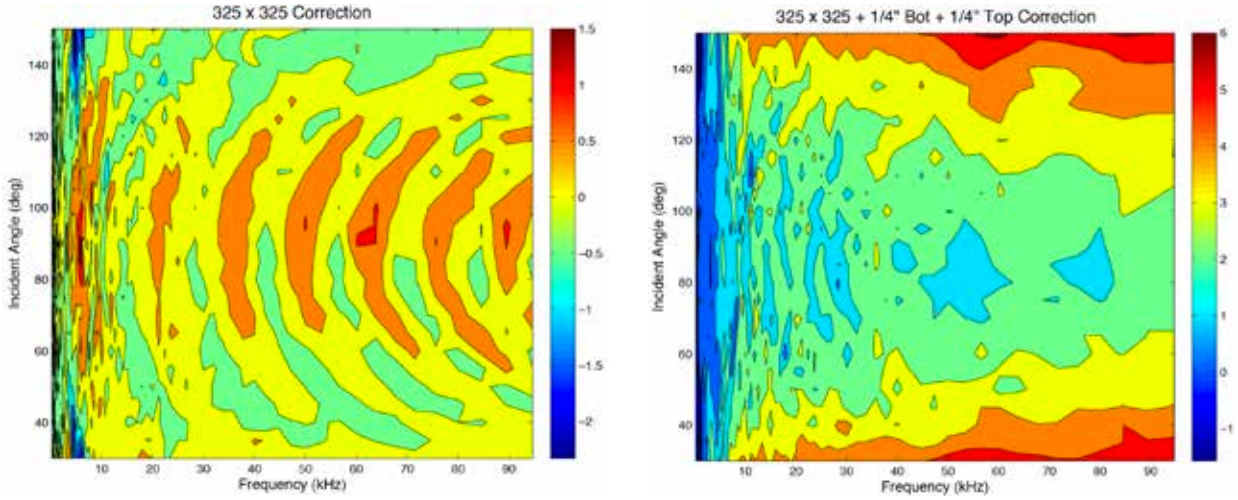

Fig. 9. ARC anechoic chamber, 48 in. source distance, plots of windscreen correction level C_{WS} for 8 in. diameter, 24 element array with:
(left) 325x325 stainless steel screen
(right) 325x325 stainless steel screen plus foam in cavity.

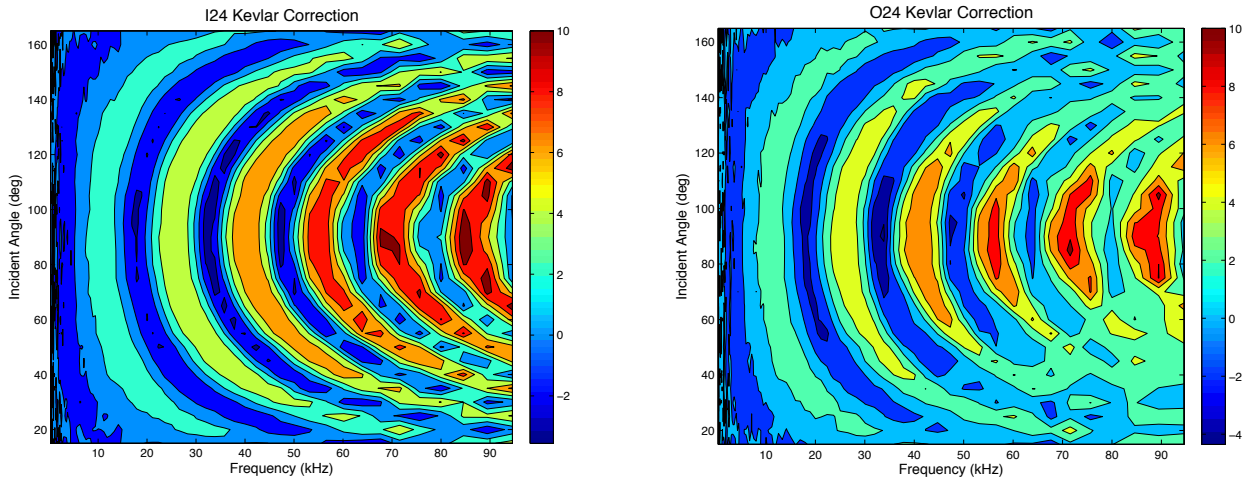

Fig. 10. ARC anechoic chamber plots (48" source distance) of windscreen correction level Cws for:
(left) Kevlar120 screen, 8" diameter, 24-element array
(right) Kevlar120 screen 23" diameter, 24-element array (2.9x scale-up of 8" diam array).

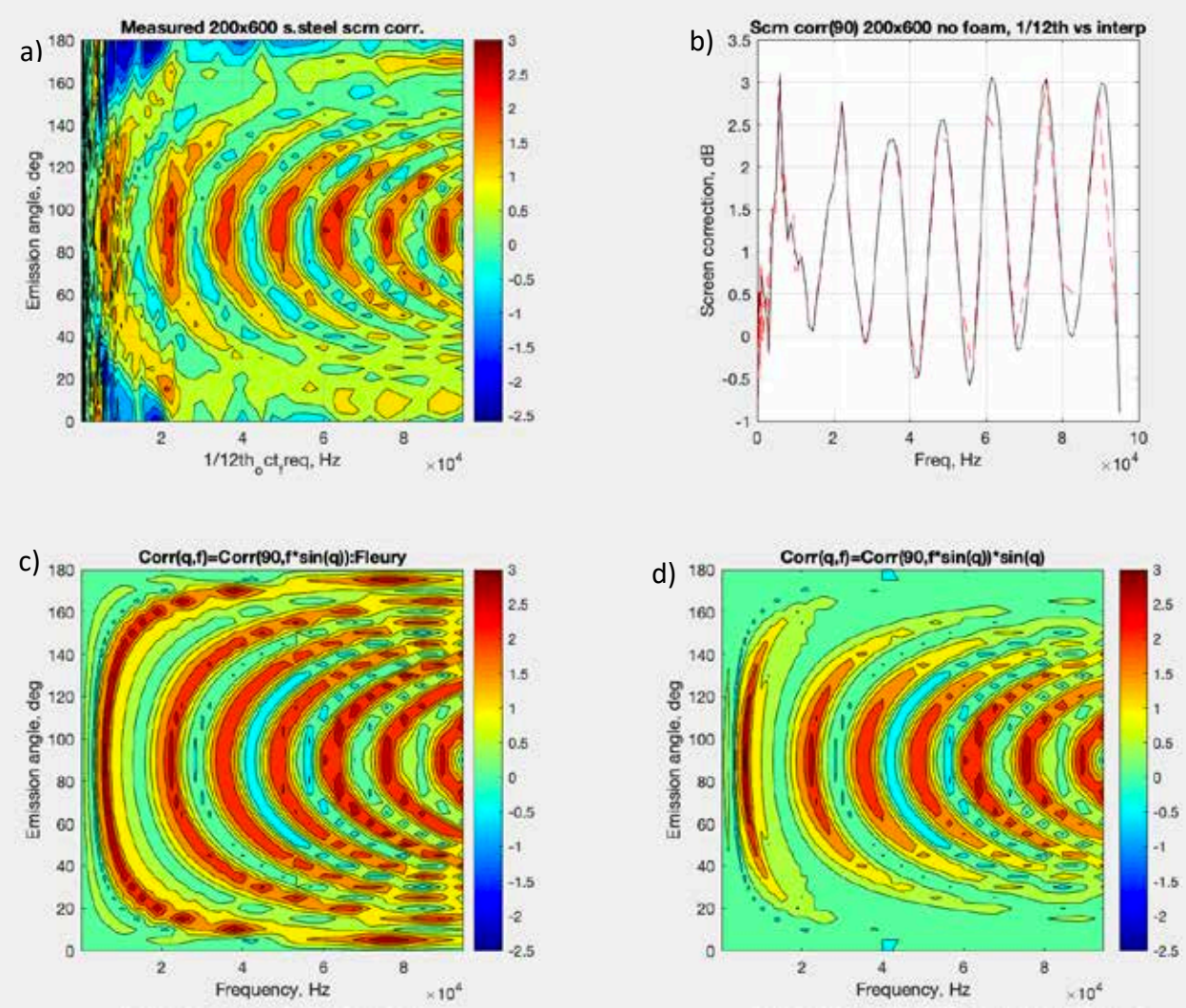

Fig. 11. Windscreen correction, Cws plots for SS200x600 (ARC anechoic chamber measurements, 48" source distance):

(a) original full correction map, 1/12th octave frequencies, 5˚ increments in θe from 0˚ to 180˚

(b) Cws spectrum at 90˚ reception(emission) angle, 1/12th octave(dashed red), interpolated (solid black)

(c) Cws map extrapolated from 90˚ spectrum: Cws(θe,f)=Cws(90˚,f*sin(θe)) (Fleury)

(d) Cws map extrapolated from 90˚ spectrum: Cws(θe,f)= sin(θe)*Cws(90˚,f*sin(θe)).

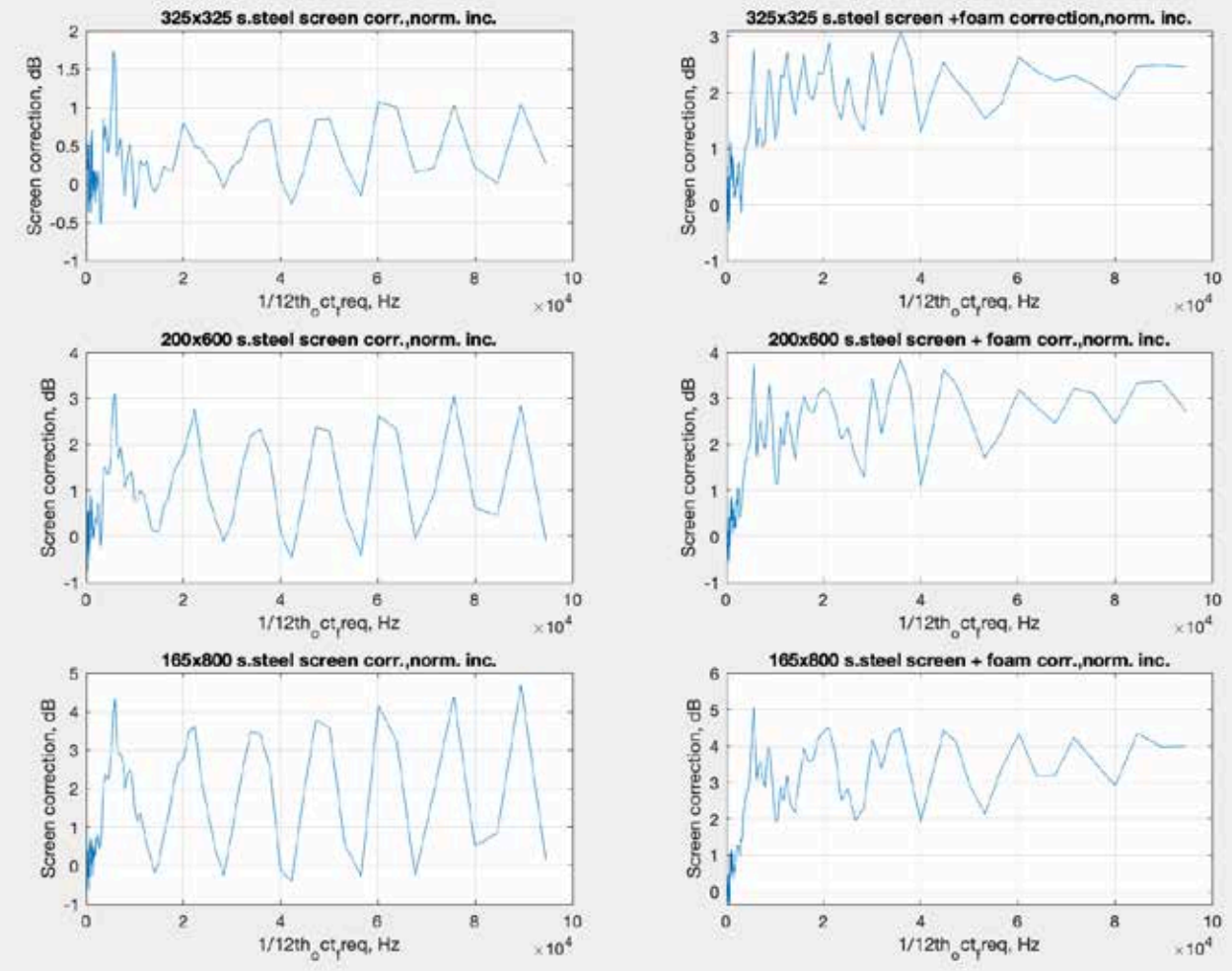

Fig. 12. Comparison of windscreen correction C_{WS} at 90˚ reception (emission) angle (θe for three stainless steel screens: 325x325 (top), 200x600(middle), and 165x800 mesh(bottom), without P30 foam insert (left plots) and with the insert (right plots) 7-by 10-Ft Wind Tunnel test at ARC.

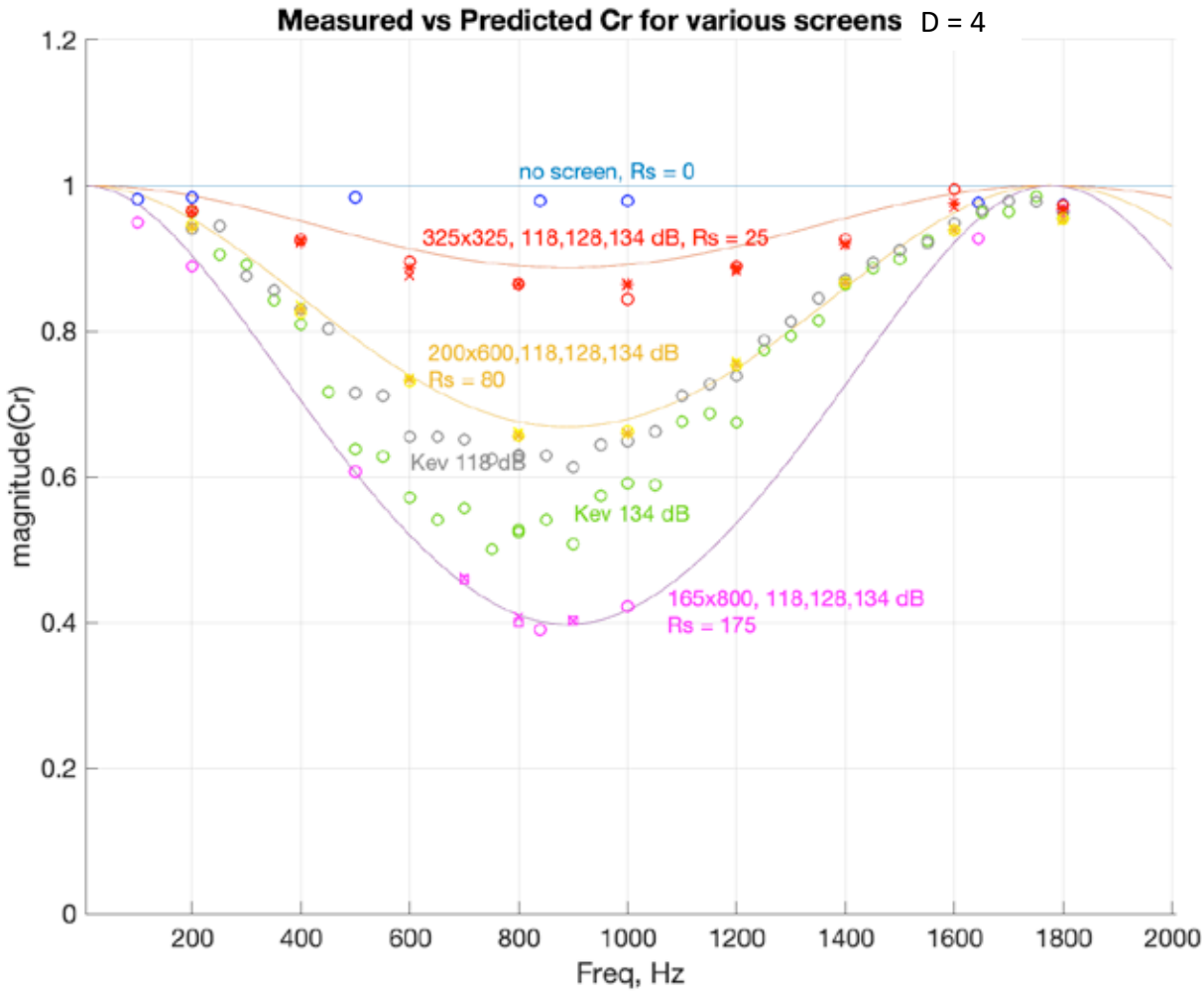

Fig. 13 Comparison of measured and predicted normal reflection coefficients C_{RN} for 4 in. diam. screen 4 in. in front of a metal plate, with effects of calibration amplitude variations of 118, 128, and 134 dB.

Magnitude Phase

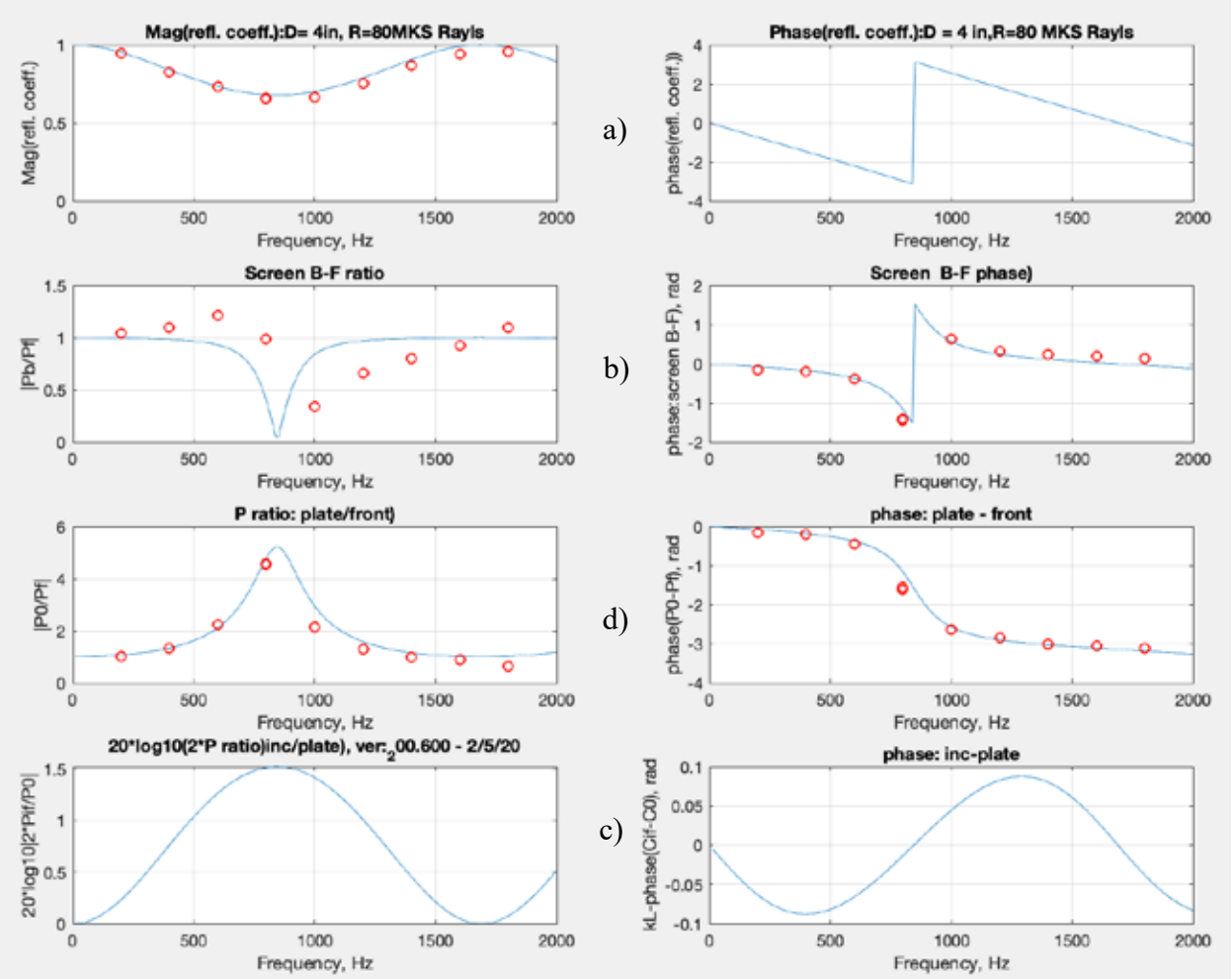

Fig. 14. Comparison of model predictions vs impedance-tube measurements of magnitudes and phases of a) reflection coefficient, b) pressure ratio: screen back to front, c) pressure ratio: plate to screen front, and d) windscreen correction. D = 4 in.